Influence of defects and doping on optical phonon lifetime and Raman linewidth in carbon nanotubes

Daner Abdula, Khoi T. Nguyen, Kwangu Kang, Scott Fong, Taner Ozel, David G. Cahill, and Moonsub Shim

Phys. Rev. B **83**, 205419 — Published 20 May 2011

DOI: 10.1103/PhysRevB.83.205419

Influence of Defects and Doping on Optical Phonon Lifetime and Raman Linewidth in Carbon Nanotubes

Daner Abdula,[1,2] Khoi T. Nguyen,[1,2] Kwangu Kang,[1,2,†] Scott Fong,[3] Taner Ozel,[2,3,‡] David G. Cahill,[1,2] and Moonsub Shim[1,2,*]

[1]*Department of Materials Science and Engineering, University of Illinois, Urbana, IL 61801*

[2]*Frederick Seitz Materials Research Laboratory, University of Illinois, Urbana, IL 61801*

[3]*Department of Physics, University of Illinois, Urbana, IL 61801*

Abstract

How doping and defects alter linewidth and lifetime of *G*-band optical phonons in carbon nanotubes is examined. Optical phonon lifetime, T_1, in thin films of nanotubes are measured by time-resolved incoherent anti-stokes Raman spectroscopy and considered along with Raman linewidths of isolated individual nanotubes. Within the doping range achievable in nanotube films in this study, T_1 does not appear to change. Varying degree of doping in individual nanotubes via electrostatic gating reveals decreasing full-width-at-half-maximum Γ down to ~4 cm^{-1} at the charge neutrality point. Increasing disorder, on the other hand, leads to a decrease in T_1 along with an increase in Γ. We observe a decrease in T_1 of ~0.4 ps at an estimated effective crystallite size L_a ~ 130 nm based on *D*-band to *G*-band peak intensity ratio. In the limit of zero-doping and zero-defects, the measured Γ of single semiconducting nanotubes coincide with lifetime broadening of ~4 cm^{-1} based on measured T_1 of 1.2 ps. Samples displaying different degree of metallic/semiconducting contributions in their static Raman spectrum are also compared and are shown to exhibit similar values of T_1.

PACS numbers: 63.20.K-, 63.22.Gh, 78.47.je

†Current affiliation: *School of Mechanical Engineering, Yonsei University, Seoul, Korea, 120-749*

‡Current affiliation: *Laboratory of Chemical Physics, National Institutes of Health, Bethesda, MD 20892*

*Corresponding author: mshim@illinois.edu

I. INTRODUCTION

Implementation of carbon nanotubes into micro- and nano-electronics has shown promise[1-3] with realistic performance limits now beginning to be established.[4] In the high-bias regime, current in nanotubes can be limited by carrier scattering with optical phonons (OPs).[5,6] In graphite, over 90% of the energy of photoexcited hot carriers are estimated to dissipate via OPs[7] and similar carrier relaxation pathways are expected in carbon nanotubes. Hence, monitoring non-equilibrium OP population dynamics can provide insights important for carbon nanotube-based electronic and optoelectronic devices. Dynamics of OPs may be affected by doping, nanotube type (metallic or semiconducting), and defects. Electron-phonon coupling (EPC) is in general important in how carriers relax and may also be an important factor in OP decay.[8] In carbon nanotubes, EPC leads to large differences in the *G*-band linewidths of metallic and semiconducting nanotubes. Metallic carbon nanotubes exhibit broadened and softened lower frequency *G*-band mode (LO mode) due to presence of a Kohn anomaly near the Dirac point.[9, 10] Doping via electrostatic gate potential or charge transfer, without introducing impurities within

the lattice, has been shown to vary this width.[11-13] Therefore, doping and metallic versus semiconducting character may be expected to cause changes in OP dynamics. However, similar or only slightly different OP population lifetimes of *G*-band phonons in metallic and semiconducting nanotubes have been measured.[14]

Defects are also important to consider in OP dynamics since lattice imperfections break crystal translational symmetry and relax momentum conservation requirement.[15-17] How defects alter OP dynamics has been investigated in crystalline materials, including III-V and II-VI compound semiconductors, and graphite.[8, 16-21] One consequence of defects on OPs can be a change in the Raman linewidth. In carbon nanotubes, specifically in metallic nanotubes, introduction of defects/disorder leads to removal of line broadening due to the presence of Kohn anomaly which counteracts line broadening by defects.[22] Defect induced broadening of Raman *G*-band can be observed in semiconducting nanotubes as well as in metallic nanotubes that have their Fermi level shifted away from the Dirac point.[23] The spectral linewidth (the full-width-at-half-maximum, Γ) is, however, related to the overall dephasing time T_2 by $\Gamma = (\pi c T_2)^{-1}$ and T_2 consists of contributions from non-equilibrium phonon population extinction, T_1, as well as pure dephasing, τ_{ph}, expressed as $2/T_2 = 1/T_1 + 1/\tau_{ph}$.[24]

Time-resolved incoherent anti-Stokes Raman scattering (TRIARS) measurements have recently been used to directly measure T_1 of *G*-band OPs. While the measured T_1 value 1.2 ps (or lifetime broadening of 4.4 cm^{-1})[14, 25, 26] is compatible with typically reported single nanotube linewidth Γ of ~ 6 – 12 cm^{-1},[27] the larger Γ from static Raman spectra suggest possible additional pure dephasing process or inhomogenous broadening to be present even in single nanotube measurements.[26] However, relatively high energy pump beam used in TRIARS, which places the system under investigation far from equilibrium, may lead to OP lifetimes that may be different

than what may be deduced from linewidths measured near equilibrium situations.[7] Time-resolved coherent anti-Stokes Raman scattering (TRCARS) studies have also been carried out to measure T_2 but seemingly conflicting results with respect to how extrinsic factors affect overall OP dephasing in carbon nanotubes have been reported.[25, 28] For single-walled carbon nanotube films on glass, one study has reported $T_2/2 = 1.1 \pm 0.1$ ps in two samples with a large difference in *D*-band intensities suggesting defects to have negligible effects.[28] However, a more recent study using a combination of TRCARS and TRIARS has shown that much smaller perturbations in the form of non-covalent interactions between nanotubes can significantly alter $T_2/2$ (while T_1 remains unaffected).[25] Ensemble samples containing both metallic and semiconducting nanotubes may cause additional complications. Therefore, a systematic study that sorts out effects of doping, defects, and nanotube type is necessary to elucidate OP dynamics.

In this work, we examine how *G*-band OP liftetime and Raman linewidth in carbon nanotubes are affected by varying doping, metallic vs. semiconducting character, and defect density. OP lifetimes are measured by TRIARS and compared to linewidth of individual nanotubes. Degree of doping is controlled either by electrostatic gate potential in the case of single nanotubes or by molecular adsorption that leads to charge transfer for thin films of nanotubes. Defect density, or the degree of disorder, is varied by annealing and covalent functionalization. A comparison between samples exhibiting high metallic and predominantly semiconducting contributions to the Raman signal is also carried out.

II. EXPERIMENTAL DETAILS

Samples were made from either carbon nanotubes prepared by high pressure carbon monoxide (HiPCO) process (Carbon Nanotechnologies Inc.) or by arc-discharge (CarboLex Inc.). Approximately 2 mg of both starting materials separately were first acid treated by sonication in 20 mL of 8 M HNO_3 for 1 h at 50 ^oC, centrifuged, washed with deionized water, centrifuged again and finally dispersed in ethanol by sonicating for 1 h at room temperature. All centrifugation steps were carried out for 30 s at 3300 rpm (1380 g). For arc-discharge nanotubes, which exhibit a significant *D*-band before and after the acid treatment, different annealing steps were taken to vary the degree of disorder. HiPCO nanotubes exhibit relatively small *D*-band and therefore the defect concentration was varied by covalent functionalization.

After the acid treatment, arc-discharge nanotubes were spin coated onto SiO_2/Si substrates with markers (300 nm oxide, markers are areas of oxide patterned and etched with reactive-ion etching prior to nanotube deposition) from the ethanol suspension. The sample where no further processing was carried out after this step is referred to as "Arc(As Prep.)". The sample that was annealed at 400 ^oC for 1 h under 500 cm^3/min flow of Ar after deposition on substrate is termed "Arc(Ar)". In order to further reduce defect concentration, another sample was heated to 350 ^oC in air then cooled to room temperature upon reaching 350 ^oC. This sample is called "Arc(Air)".

HiPCO nanotube samples were covalently functionalized by mixing acid-treated tubes suspended in ethanol (~0.1 mg/mL) with 20 mM, 100 mM, or 200 mM aqueous solution of 4-nitrobenzene diazonium tetrafluoroborate (4-NBDT, Fluka) in 1:1 volume ratio; sonicating for 1 min; allowing the reaction to go on for 20 min; centrifuging and rinsing the nanotubes with deionized water; centrifuging and re-suspending them in ethanol. These suspensions were then used to spin coat nanotubes onto markered substrates. These samples are labeled "HiPCO(10

mM)", "HiPCO(50 mM)", and "HiPCO(100 mM)" according to the concentration of 4-NBDT after mixing nanotube and functionalizing solutions. A fourth sample, "HiPCO(0 mM)", was made in the same manner, but distilled water without 4-NBDT was used to make the 1:1 reaction mixtures. After OP lifetime measurements were carried out, these four samples were exposed to high molecular weight poly(ethylenimine) (PEI, Sigma) for doping purposes. Neat PEI was spin coated on the samples and allowed to adsorb for 1 h, then thoroughly rinsed with distilled water to remove excess PEI. Samples doped as such are noted along with the concentration of 4-NBDT they were functionalized with previously [e.g., "HiPCO(100 mM/PEI)"]. Finally, a last sample of non-functionalized HiPCO nanotubes on-substrate [prepared in the same manner as HiPCO(0 mM)] was annealed at 400 ^{o}C for 1 h under 500 cm^3/min flow of Ar and is called "HiPCO(Ar)".

The above arc-discharge and HiPCO samples of ensemble/bundles of nanotubes are collectively referred to as "thin film samples." For single nanotube and device measurements, carbon nanotubes were grown directly on Si/SiO_2 substrates by chemical vapor deposition using ferritin catalyst and CH_4/H_2 following Ref. 12. Electrical contacts to individual carbon nanotubes were made by patterning 35 nm thick Au electrodes with 5 nm Ti wetting layer on top of the nanotubes. Electrochemical gate potential was applied to these contacted nanotube devices using a 20 wt% $LiClO_4 \cdot H_2O$ in PEI.

Static Raman spectroscopy was carried out on a Jobin Yvon LabRam HR 800 micro-Raman spectrometer with a 785 nm laser excitation source (75 W/cm^2 intensity unless otherwise noted) and a 50X air objective providing a spot size with a $1/e^2$ radius of 1.5 μm. A mode-locked Ti:sapphire laser with an 80 MHz repetition rate was used for TRIARS measurements.[14, 29] Total laser fluence was 58.3 μJ/cm^2 (unless otherwise noted) and the pump:probe power ratio was kept at 3:2. Pump and probe beams were cross polarized and focused with a 20X air objective to a

spot size with a $1/e^2$ radius of 3.75 μm. A central wavelength of 787 nm with a full-width-at-half-maximum of ~10 nm was used. A 785 nm laser line filter was used for the probe beam and a 790 nm long-pass filter was used for the pump to prevent Raman signal from the pump interfering with that from the probe. The Raman scattered light was collected in a spectrograph consisting of a diffraction grating and a thermoelectrically cooled CCD array. The OP population lifetimes were obtained by fitting the data collected to a convolution of the pump-probe correlation with a response function of abrupt rise followed by an exponential decay. Pump-probe correlation was measured by two-photon absorption in a GaP detector.

III. SAMPLE PROCESSING EFFECTS ON DOPING, METALLIC/SEMICONDUCTING CHARACTER, AND DEFECT CONCENTRATION

Static Raman spectroscopy is a useful tool to determine relative degree of doping, metallic/semiconducting character, and defect concentration of each sample type. Relative defect concentration can be estimated using a ratio of integrated area of the *D*-band to that of the *G*-band (A_D/A_G).[23] The relative degree of doping can be inferred from shifts in the *D*-band. With strong coupling of OPs to carrier excitations, the *G*-band shifts symmetrically (or nearly symmetrically) with respect to carrier concentration and cannot be used to distinguish *p*- or *n*-type doping.[11-13] The *D*-band (as well as the 2D band), on the other hand, shows a monotonic decrease in frequency from *p*-type to *n*-type[30] and is therefore used here to determine relative doping levels. Note that, throughout this paper, we refer to doping specifically as increasing the number of carriers, either by charge transfer or by electrostatic gating, without the introduction of impurities and therefore defects/disorder into the lattice. Raman peak frequencies and A_D/A_G

ratios are acquired by fitting the obtained Raman spectra, examples of which are shown in Fig. 1. HiPCO samples are fitted with one Lorentzian for the *D*-band and two Lorentzians for the *G*-band. This *G*-band lineshape combined with RBM frequencies observed indicates that predominantly semiconducting nanotubes contribute to the Raman spectra of HiPCO tubes at the laser energy of 1.58 eV (785 nm) used here. Spectra of arc-discharge samples are fitted with one Lorentzian for the *D*-band and two Lorentzians and a Fano line (horizontal hatches) for the *G*-band to account for EPC effects in metallic nanotubes.[12] Based on the ratio of integrated intensities of the Fano line and the total *G*-band, A_{Fano}/A_G, for all arc-discharge nanotube samples, we estimate metallic tube contribution to the Raman signal to be about 35%. This value does not change with the degree of disorder as shown in Fig. 1(b).

The degree of doping, on the other hand, does change with disorder induced by covalent functionalization with 4-NBDT. HiPCO samples show that functionalization with 4-NBDT leads to *p*-type doping as inferred from the *D*-band frequency up-shift[30] along with increasing A_D/A_G, as quantified in Fig. 2. We expect disorder contribution to *D*-band frequency shift to be significantly smaller than the doping contribution in the 4-NBDT functionalized HiPCO samples based on measurements on single nanotubes where a *D*-band frequency shift of only ~1 cm^{-1} has been observed at different defect densities (A_D/A_G from < 0.1 to ~0.5 with laser excitation at 633 nm) when charge neutrality has been ensured with electrochemical gate potential (data not shown). Because of the concurrent doping and defect density increase, PEI is used as a "counter-dopant" to separate out the two effects. PEI adsorption does not change A_D/A_G.[31] Note, however, that annealing in Ar decreases the defect concentration. For arc-discharge nanotubes, which start with a higher degree of defects, different annealing processes are carried out to vary defect concentration. Annealing causes only minor changes in the degree of doping (*D*-band frequency

change of 2 cm^{-1} or less). Both annealing and covalent functionalization do not alter the distribution of nanotube types (semiconducting and metallic) and diameters as verified by radial breathing modes (RBMs) measured across all specimens.

IV. POTENTIAL LASER-INDUCED SAMPLE DAMAGE AND HEATING

Before discussing TRIARS measurements of OP lifetimes, possible laser-induced damage and heating need to be considered. This is especially important since introduction of defects in graphitic materials is known to lower thermal conductivity,[32, 33] which can then enhance laser heating and damage. Laser-induced damage can be easily monitored by examining A_D/A_G ratio in the Raman spectrum. Raman spectra of our most defective/functionalized (and therefore least thermally conductive) sample after PEI doping, HiPCO(100 mM/PEI), shows no increase in A_D/A_G after TRIARS measurements and laser heating measurements (discussed below) where laser intensity was varied up to the maximum used in all experiments here. Therefore, we conclude that we are in a regime where laser damage is negligible.

Even in the absence of actual damage, laser irradiation of carbon nanotubes may cause sample heating, which is known to change the phonon lifetime.[14] Raman thermometry can be used to determine the degree of laser induced heating through frequency shifts of the *G*-band.[34] Static Raman measurements with the sample mounted on a heating stage under Ar are carried out to calibrate G^+ peak shift with temperature. From Fig. 3(a), we determine $-0.033 cm^{-1}/K$, similar to the slope for graphene in Ref. 34. Figure 3(b) shows G^+ peak frequencies at different laser intensities for HiPCO(0 mM) and HiPCO(100 mM/PEI) samples. Even for our most defective sample under laser intensities higher than those used for TRIARS measurements, no down-shift

in the G^+ peak frequency is observed. Therefore, we expect laser heating to have a negligible effect in sample temperature increase (< ~20 K based on our spectral resolution of 0.7 cm^{-1}). Given the assumption that lifetime scales inversely with temperature,[29] this upper limit in laser-induced temperature increase leads to less than ~6 % change in T_1. Furthermore, we have also measured T_1 at multiple laser fluences to verify that laser heating effects are insignificant even for the sample with the highest degree of functionalization. Indeed, within our experimental error of ±0.1 ps, T_1 is the same for both half and double the usual TRIARS laser fluence used.

V. DOPING EFFECTS ON OPTICAL PHONON LINEWIDTH

Having established that, even at the highest fluence for the most defective samples, laser heating and damage are negligible, we consider now how doping affects *G*-band OP lifetime and Raman linewidth. Examples of TRIARS spectra at different time delays for HiPCO(0 mM) sample are shown in Fig. 4(a). Figure 4(b) shows the OP decay in three of the non-functionalized samples as measured by TRIARS. In Fig. 5, *G*-band OP lifetimes are plotted as a function of *D*-band frequency for all thin film samples. Note that at a fixed laser energy, higher frequency *D*-band corresponds to more *p*-type doping.[30] For arc-discharge nanotubes, annealing in air does not alter the *D*-band frequency (and therefore the degree of doping) but increases the OP lifetime slightly from 1.0 ± 0.1 ps to 1.3 ± 0.1 ps. Annealing in Ar and PEI adsorption do alter the *D*-band frequency in HiPCO nanotubes but T_1 remains the same within the experimental error. For HiPCO(10 mM), HiPCO(50 mM), and HiPCO(100 mM) samples, T_1 remains the same after PEI doping even with a *D*-band frequency difference of up to ~8 cm^{-1} (or Fermi level position

difference on the order of 1 eV).[30] However, in the latter set of functionalized samples, defects altering T_1 may prevent observation of possible doping induced changes in T_1.

In the low defect limit (i.e. non-functionalized nanotube films), doping with PEI leads to a relatively small downshift in the *D*-band frequency (< 3 cm^{-1}). A larger change in the degree of doping is likely to be necessary to ascertain whether or not there is an effect from doping. Unfortunately, dense films of bundled nanotubes used in TRIARS measurements do not exhibit significant Raman *D*-band frequency shifts upon electrolyte gating. Therefore, we consider doping dependent linewidth of individual nanotubes, which can be gated much more effectively and provide a better upper limit on homogeneous linewidths. We limit our discussion here to semiconducting nanotubes since the degree of line broadening dominated by EPC in metallic nanotubes varies from tube to tube as well as with doping. If optical phonon relaxation by carrier excitation in metallic nanotubes dominated the lifetime, typical *G*-band linewidths of several tens of cm^{-1} would also correspond to time scale beyond our temporal resolution of TRIARS measurements. Furthermore, high electronic temperature induced by the pump in TRIARS has been shown to remove EPC effects in graphite as evidenced by transient stiffening of the *G*-band[7] and we anticipate similar effects making carrier excitation induced fast decay expected in metallic nanotubes to have negligible contributions to our measured TRIARS signal. Figure 6(a) shows the gate voltage dependence of G^+ peak linewidth for a single semiconducting nanotube which does not exhibit measurable *D*-band (i.e. low defect limit). G^- peak linewidths are usually similar to those of G^+ peak and therefore we focus on higher intensity G^+ peak. At the charge neutrality point (V_G = - 0.3 V), the linewidth is the narrowest with Γ = 5 cm^{-1}, corresponding to $T_2/2$ = 1.1 ps. This value is similar to the measured OP lifetime of ~1.2 ps for low defect samples.

When electrostatic gating introduces carriers into the semiconducting nanotube, G^+ peak linewidth nearly doubles to 9.5 cm^{-1}. Static Raman spectra of the *G*-band (along with two-Lorentzian curve fits) at two indicated gate voltages are shown in Fig. 6(b). The increase in *G*-band linewidth of semiconducting nanotubes with doping has also been reported previously, with larger increase using electrolyte gate[13] (as used here) than with back gate[11] configuration due to the much higher efficiency of polymer electrolyte gating. Semiconducting nanotubes are expected to exhibit *G*-band phonon softening similar to metallic nanotubes but with a smaller degree of softening and *without* line broadening due to virtual electron-hole pair generation rather than actual carrier excitation.[11, 35] A possible origin of the broadening may be gate inducing charges near the nanotube (e.g. on substrate and/or adsorbed molecules) leading to variations in local electric fields which in turn can cause inhomogeneous broadening. Doping causing only inhomogeneous broadening and leaving the homogeneous linewidth unchanged would be consistent with doping independent T_1. Unfortunately, strongly non-equilibrium behavior expected of OPs due to the pump pulse in TRIARS prevents direct comparison of T_1 with linewidth obtained by static Raman measurements. Doping dependent Raman linewidth does, however, indicate that the observed variations in the *G*-band linewidth of individual semiconducting nanotubes (which is often reported to range between 6 to 12 cm^{-1})[27] are, at least in part, due to variations in molecular adsorption from the ambient and/or substrate induced doping/charging.[30, 36]

VI. DEFECT EFFECTS ON OPTICAL PHONON LIFETIME

While doping broadens Raman linewidth without an apparent change to T_1, we observe that defects alter both. HiPCO(0 mM) and Arc(As-Prep.) samples, whose TRIARS measurements are shown in Fig. 4(b), are prepared in the same manner here as samples reported in Ref. 14. The T_1 values measured are similar in both cases with the HiPCO sample having a slightly longer lifetime (1.0 ± 0.1 ps vs. 1.2 ± 0.1 ps). However, the difference in the degree of disorder between these two samples is significant. For HiPCO(0 mM) sample, A_D/A_G = 0.21 ± 0.03 whereas A_D/A_G = 0.56 ± 0.01 for Arc(As-Prep.) sample as shown in Fig. 1(a) and bottom spectrum in Fig. 1(b), respectively. After annealing in air, arc-discharge nanotubes show a marked decrease in A_D/A_G down to 0.11 ± 0.02 [top spectrum in Fig. 1(b)]. This reduction in defect density leads to an increase in T_1 from 1.0 ± 0.1 ps to 1.3 ± 0.1 ps, now comparable to HiPCO(0 mM). This result suggests that HiPCO and arc-discharge nanotubes, although having different degree of metallic/semiconducting contributions to the measured static Raman spectra, exhibit similar OP lifetimes. Based on pump-induced transient decoupling of OP-mediated electronic transitions observed in graphite,[7] similar OP lifetimes in metallic and semiconducting nanotubes may be expected and can explain these results. The key difference observed between HiPCO and arc-discharge tubes prior to annealing appears to be the consequence of variations in the defect concentration.

Covalent functionalization with 4-NBDT provides a more systematic way to investigate the influence of defects on OP lifetime. Figure 7(a) shows the two extremes. Functionalization of HiPCO nanotubes with 100 mM 4-NBDT decreases T_1 from 1.2 ± 0.1 ps to 0.8 ± 0.1 ps while increasing A_D/A_G from 0.21 ± 0.03 to 1.53 ± 0.17. The dependence of T_1 on A_D/A_G for all thin film samples studied is shown in Fig. 7(b). The corresponding lifetime broadening, defined here as $(2\pi c T_1)^{-1}$, is shown in Fig. 8. In order to compare to reported correlation between defect

density and D to G ratio,[37-41] data in Fig. 8 are plotted using D-band and G-band peak height ratios, I_D/I_G, rather than the integrated intensity ratios. Using integrated intensity ratios leads to the same trend. Based on Ref. 38, where defect concentrations were estimated from thermogravimetric analysis of 4-NBDT functionalized nanotubes, we estimate the sample with maximum disorder to have defect density of ~1 defect per 50 lattice C atoms.[42] Using a more widely used relation for nanographitic materials,[37, 39-41] we calculate crystallite size L_a ~ 130 nm from which we estimate defect density of ~1 defect per 300 lattice C atoms.[43] Taking the average of these two values, we estimate ~1 defect per 175 lattice C atoms to cause 0.4 ps decrease in T_1 or a change in lifetime broadening of ~2 cm^{-1}.

Figure 8 also compares the G^+ peak linewidth Γ of individual semiconducting nanotubes with lifetime broadening of thin film samples. Both increase approximately linearly with defect density. The static Raman linewidth of single nanotubes exhibits stronger dependence on I_D/I_G but this may be a consequence of defect induced inhomogeneous broadening.[17, 19, 44, 45] However, in the limit of zero-defects for charge neutral nanotubes, Γ and lifetime broadening converge. Note that the slight offset for the filled squares at I_D/I_G = 0 is likely to be arising from doping/charging as discussed in the previous section. The open squares are from electrochemically gated nanotubes where zero-doping is ensured. These data points therefore provide a better upper limit on the homogeneous linewidth.

While the convergence of Γ and lifetime broadening at zero-charge and zero-doping limit can imply that T_1 dominates the overall dephasing time in nanotubes, effects of high transient electronic temperature induced by the pump beam in the TRIARS measurements need to be considered before such conclusions can be made. In graphite, the high electronic temperature has been shown to lead to an equivalent effect as gate shifting the Fermi level away from the Dirac

point and OP relaxation via carrier excitation becomes no longer accessible or less likely.[7] The measured T_1 of 2.2 ~ 2.4 ps in Refs. 7 and 31 is in reasonable agreement with calculated lifetime based on anharmonic decay, mainly into two acoustic phonons. In graphene, a faster T_1 of ~ 1.2 ps has been suggested to arise from coupling to the substrate.[29] Carbon nanotubes also exhibit similar faster T_1 of ~1.2 ps but the substrate is not likely to be providing additional decay paths. In the relatively thick films of nanotubes used here and in Ref. 14, the majority of the nanotubes are not directly supported by the substrate. Furthermore, nanotubes suspended in D_2O exhibit similar T_1 of 1.1 ps.[26] The similar value of T_1 for bundles of nanotubes on substrate and isolated nanotubes dispersed in solution also indicates that that contacts between nanotubes are not important in the measured OP lifetime. TRIARS measurements are carried out with OP population far from equilibrium and the decay rate observed may be different than that expected of near-equilibrium situation and therefore comparison to linewidth obtained through static Raman measurements may be problematic. However, slower, rather than faster, OP relaxation is expected far from equilibrium as shown in bilayer graphene and graphite[46] and as suggested by a slight decrease in T_1 with decreasing pump power in carbon nanotubes.[14] Even if we assume zero-doping, zero-charge limit Γ of 4 ~ 5 cm^{-1} giving only an upper limit for homogeneous linewidth, imposing that the pump in TRIARS measurements causes measured T_1 values to be larger than the actual (or near-equilibrium) lifetime would lead to an unreasonable result of lifetime broadening being larger than the homogeneous width. One possible explanation of observed T_1 in carbon nanotubes being faster than the expected anharmonic decay rates in graphene and graphite is coupling of *G*-band mode to RBM phonons.[47] Since this decay path is accessible only when the nanotube is photoexcited, near-equilibrium OP lifetime can be expected to be longer in this case. Then, Γ ~ 4 cm^{-1} from static Raman measurements must include

additional decay path, dephasing process or inhomogeneous broadening. However, it appears somewhat fortuitous that any of these processes should lead to the near-equilibrium linewidth being same as lifetime broadening that includes an unrelated anharmonic decay into RBM phonon far from equilibrium. Whether or not the convergence of Γ and lifetime broadening is an unrelated coincidence remains an open question.

Decreasing T_1 with defects observed in Fig. 7(b) is surprising in that defects have been shown to have little or no effect on OP lifetimes in other materials.[44, 45] In graphene, conflicting results exist where both I_D/I_G dependent[48] and independent[46] OP lifetimes have been reported. Point defects are often considered to cause elastic scattering of phonons and therefore the rates of anharmonic decay into lower energy phonons are not expected to be altered.[8, 49] However, 4-NBDT molecules used here introduce relatively large nitrophenyl groups chemisorbed on the sidewalls of nanotubes and hence may not be treated as simple point defects. The combination of adsorbed chemical groups and lattice disorder induced by functionalization with 4-NBDT may lead to additional relaxation pathways. Existing defects can also enhance reactivity of neighboring lattice atoms,[50, 51] and therefore the distribution of functional groups and disorder in the lattice may not be uniform which may further facilitate OP relaxation.

VII. CONCLUSIONS

By varying the doping level in individual semiconducting carbon nanotubes using polymer electrolyte gating, we have shown that Raman *G*-band linewidth as narrow as ~4 cm^{-1} can be observed at the charge neutrality point. Variations in molecular adsorption from the ambient and/or substrate induced doping/charging may be the main reason for larger values and

variations in linewidths (6 – 12 cm^{-1}) often reported. Optical phonon lifetime does not change within the doping range achievable here for thin films of nanotubes. Increasing disorder, on the other hand, alters both linewidth and the lifetime. Lifetime broadening inferred from measured T_1 and linewidth Γ measured by static Raman both scale linearly with I_D/I_G with the latter having a stronger dependence likely due to inhomogeneous broadening caused by covalent functionalization. In the limit of zero-doping and zero-defects, the measured Γ of single semiconducting nanotubes coincide with lifetime broadening expected from measured T_1 of 1.2 ps. By reducing the degree of defect induced changes on the observed OP lifetime, we have also shown that samples displaying different degree of metallic/semiconducting character exhibit similar T_1 value of ~1.2 ps.

ACKNOWLEDGEMENTS

This material is based upon work supported by the NSF (Grant No. 09-05175). Experiments were carried out in part in the Frederick Seitz Materials Research Laboratory Central Facilities, University of Illinois, which are partially supported by the U.S. Department of Energy under Grants No. DE-FG02-07ER46453 and No. DE-FG02-07ER46471.

REFERENCES

[1] S. J. Tans, A. R. M. Verschueren, and C. Dekker, Nature **393**, 49 (1998).
[2] J. Kong, N. R. Franklin, C. Zhou, M. G. Chapline, S. Peng, K. Cho, and H. Dai, Science **287**, 622 (2000).
[3] D. Abdula and M. Shim, ACS Nano **2**, 2154 (2008).
[4] X. Zhou, J. Y. Park, S Huang, J. Liu, and P. L. McEuen, Phys. Rev. Lett. **95**, 146805 (2005).
[5] Z. Yao, C. L. Kane, and C. Dekker, Phys. Rev. Lett. **84**, 2941 (2000).

[6] V. Perebeinos, J. Tersoff, and P. Avouris, Phys. Rev. Lett. **94**, 086802 (2005).
[7] H. Yan, D. Song, K. F. Mak, I. Chatzakis, J. Maultzsch, and T. F. Heinz, Phys. Rev. B **80**, 121403(R) (2009).
[8] N. Del Fatti, F. Ganikhanov, P. Langot, R. Tommasi, and F. Vallee., J. Nonlinear Opt. Phys. Mater. **7**, 271 (1998).
[9] Y. Wu, J. Maultzsch, E. Knoesel, B. Chandra, M. Huang, M. Y. Sfeir, L. E. Brus, J. Hone, and T. F. Heinz, Phys. Rev. Lett. **99**, 027402 (2007).
[10] S. Piscanec, M. Lazzeri, F. Mauri, A. C. Ferrari, and J. Robertson, Phys. Rev. Lett. **93**, 185503 (2004).
[11] J. C. Tsang, M. Freitag, V. Perebeinos, J. Liu, and Ph. Avouris, Nat. Nanotechnol. **2**, 725 (2007).
[12] K. T. Nguyen, A. Gaur, and M. Shim, Phys. Rev. Lett. **98**, 145504 (2007).
[13] A. Das, A. K. Sood, A. Govindaraj, A. M. Saitta, M. Lazzeri, F. Mauri, and C. N. R. Rao, Phys. Rev. Lett. **99**, 136803 (2007).
[14] K. Kang, T. Ozel, D. G. Cahill, and M. Shim, Nano Lett. **8**, 4642 (2008).
[15] J. Petzelt and N. Setter, Ferroelectrics **150**, 89 (1993).
[16] R. Cusco, E. Alarcon-Llado, J. Ibanez, L. Artus, J. Jimenez, B. Wang, and M. J. Callahan, Phys. Rev. B **75**, 165202 (2007).
[17] M. Millot, R. Tena-Zaera, V. Munoz-Sanjose, J. Broto, and J. Gonzalez, Appl. Phys. Lett. **96**, 152103 (2010).
[18] S. Anand, P. Verma, K. P. Jain, and S. C. Abbi, Physica B **226**, 331 (1996).
[19] L. Bergman, D. Alexson, P. L. Murphy, R. J. Nemanich, M. Dutta, M. A. Stroscio, C. Balkas, H. Shin, and R. F. Davis, Phys. Rev. B **59**, 12977 (1999).
[20] K. Ishioka, M. Hase, M. Kitajima, and K. Ushida, Appl. Phys. Lett. **78**, 3965 (2001).
[21] K. Ishioka, M. Hase, K. Ushida, and M. Kitajima, Appl. Surf. Sci. **197**, 726 (2002).
[22] K. T. Nguyen and M. Shim, J. Am. Chem. Soc. **131**, 7103 (2009).
[23] D. Abdula, K. T. Nguyen, and M. Shim, J. Phys. Chem. C **111**, 17755 (2007).
[24] S. F. Fischer, and A. Laubereau, Chem. Phys. Lett. **35**, 6 (1975).
[25] Y. J. Lee, S. H. Parekh, J. A. Fagan, and M. T. Cicerone, Phys. Rev. B **82**, 165432 (2010).
[26] D. Song, F. Wang, G. Dukovic, M. Zheng, E. D. Semke, L. E. Brus, and T. F. Heinz, Phys. Rev. Lett. **100**, 225503 (2008).
[27] A. Jorio, A. G. Souza Filho, G. Dresselhaus, M. S. Dresselhaus, A. K. Swan, M. S. Unlu, B. B. Goldberg, M. A. Pimenta, J. H. Hafner, C. M. Lieber, and R. Saito, Phys. Rev. B **65**, 155412 (2002).
[28] K. Ikeda and K. Uosaki, Nano Lett. **9**, 1378 (2009).
[29] K. Kang, D. Abdula, D. G. Cahill, and M. Shim, Phys. Rev. B **81**, 165405 (2010).
[30] M. Shim, A. Gaur, K. T. Nguyen, D. Abdula, and T. Ozel, J. Phys. Chem. C **112**, 13017 (2008).
[31] M. Shim, T. Ozel, A. Gaur, and C. Wang, J. Am. Chem. Soc. **128**, 7522 (2006).
[32] C. N. Hooker, A. R. Ubbelohde, F. R. S. and D. A. Young, Proc. R. Soc. A **276**, 83 (1963).
[33] P. G. Klemens and D. F. Pedraza, Carbon **32**, 735 (1994).
[34] D. Abdula, T. Ozel, K. Kang, D. G. Cahill, and M. Shim, J. Phys. Chem. C **112**, 20131 (2008).
[35] A. Das and A. K. Sood, Phys. Rev. B **79**, 235429 (2009).
[36] A. Gaur and M. Shim, Phys. Rev. B **78**, 125422 (2008).

[37] Z. H. Ni, L. A. Ponomarenko, R. R. Nair, R. Yang, S. Anissimova, I. V. Grigorieva, F. Schedin, P. Blake, Z. X. Shen, E. H. Hill, K. S. Novoselov, and A. K. Geim, Nano Lett. **10**, 3868 (2010).
[38] J. Stephenson, J. L. Hudson, A. D. Leonard, B. K. Price, and J. M. Tour, Chem. Mater. **19**, 3491 (2007).
[39] L. G. Cancado, K. Takai, T. Enoki, M. Endo, Y. A. Kim, H. Mizusaki, A. Jorio, L. N. Coelho, R. Magalhaes-Paniago, and M. A. Pimenta, Appl. Phys. Lett. **88**, 163106 (2006).
[40] N. Soin, S. S. Roy, S. C. Ray, and J. A. McLaughlin, J. Raman Spectrosc. **41**, 1227 (2010).
[41] J. H. Chen, W. G. Cullen, C. Jang, M. S. Fuhrer, and E. D. Williams, Phys. Rev. Lett. **102**, 236805 (2009).
[42] In Ref. 38, a 633 nm laser was used whereas we have used a 785 nm source. To estimate defect density measured by 785 nm laser source, we multiply our measured I_D/I_G by (633 nm/785 nm)^4 to account for the laser wavelength to the 4th power dependence.
[43] The relation $L_a(\text{nm}) = (2.4\times10^{-10})\lambda^4(nm) \times (I_D/I_G)^{-1}$ is used to obtain crystallite size L_a which takes into account excitation wavelength λ. Approximating a circular crystallite shape, the number of functional groups per lattice carbon atom can be estimated as: $\#/C = [2\pi(L_a/2)/(a_{C\text{-}C}\times\cos(30^o))]/[\rho\times\pi(L_a/2)^2]$ where $a_{C\text{-}C}$ is the C-C bond length and ρ is carbon atom density of graphene, which reduces to $\#/C = 3a_{C\text{-}C}/L_a$. This equation treats the circumference of the crystallite as being entirely functionalized and therefore the ratio of the number of atoms along the circumference to those within the area of the crystallite equals $\#/C$.
[44] K. T. Tsen and H. Morkoc, Phys. Rev. B **37**, 7137 (1988).
[45] J. A. Kash, S. S. Jha, and J. C. Tsang, Phys. Rev. Lett. **58**, 1869 (1987).
[46] H. Wang, J. H. Strait, P. A. George, S. Shivaraman, V. B. Shields, M. Chandrashekhar, J. Hwang, F. Rana, M. G. Spencer, C. S. Ruiz-Vargas, and J. Park, Appl. Phys. Lett. **96**, 081917 (2010).
[47] A. Gambetta, C. Manzoni, E. Menna, M. Meneghetti, G. Cerullo, G. Lanzani, S. Tretiak, A. Piryatinski, A. Saxena, R. L. Martin, and A. R. Bishop, Nat. Phys. **2**, 515 (2006).
[48] J. M. Dawlaty, S. Shivaraman, M. Chandrashekhar, F. Rana, and M. G. Spencer, Appl. Phys. Lett. **92**, 042116.
[49] M. Hase and M. Kitajima, J. Phys.: Condens. Matter **22**, 073201 (2010).
[50] C. Wang, G. Zhou, J. Wu, B. Gu, and W. Duan, Appl. Phys. Lett. **89**, 173130 (2006).
[51] Y. Fan, B. R. Goldsmith, and P. G. Collins, Nat. Mater. **4**, 906 (2005).

Figure Captions

FIG. 1. (Color online) Raman spectra of non-functionalized HiPCO nanotubes, "HiPCO(0 mM)" (a), and argon and air annealed arc-discharge samples, "Arc(Ar)" and "Arc(Air)", respectively (b), along with examples of curve fitting. Grey lines are the curve fitting results and the red curves are the components of the fit. Ratios of the Fano peak (shaded red) integrated intensity to that of the *G*-band (A_{Fano}/A_G) for characterizing metallic nanotube content and relative disorder (A_D/A_G) for arc-discharge nanotubes are also noted. Spectra in (b) are offset for clarity.

FIG. 2. Relative disorder (defined as integrated intensity ratio of *D*-band to *G*-band, A_D/A_G) and *D*-band frequency (representing relative degree of doping) of functionalized (4-NBDT solution concentration in mM), Ar-annealed, and PEI doped HiPCO samples. Error bars (some smaller than the symbols) are obtained from average of spectra collected at three different locations of each sample. Connecting lines are guides to the eye.

FIG. 3. (Color online) (a) Temperature dependence of G^+ peak frequency obtained for HiPCO(0 mM) sample measured by heating the substrate and probing with low intensity (127 W/cm^2) HeNe laser. Circles and squares correspond to two different heating cycles. A value of $d\omega/dT = -0.033$ cm^{-1}/K is obtained. (b) Effects of laser intensity on G^+ peak frequency of HiPCO(0 mM) and HiPCO(100 mM/PEI) samples. "Min" and "Max" refer to the minimum and maximum TRIARS laser intensities used to verify that laser heating and damage are negligible. "Std." is the

value of intensity used for all other TRIARS measurements (I = 7.9 kW/cm^2). Relative disorder, A_D/A_G, remains the same after laser power dependence and TRIARS measurements even for the most defective sample, HiPCO(100 mM/PEI).

FIG. 4. (Color online) (a) Examples of background (signal at delay stage position of t = -10ps) subtracted TRIARS spectra. (b) Normalized integrated TRIARS intensity (I/I_{max}) as a function of probe delay for Arc(As Prep), Arc(Air), and HiPCO(0 mM) samples with A_D/A_G of 0.56 ± 0.01, 0.11 ± 0.02, and 0.21 ± 0.03 respectively. Pump-probe correlation is also shown.

FIG. 5. (Color online) OP lifetime, T_1, vs. D-band frequency for non-functionalized (square), functionalized (filled circle), and functionalized/PEI-doped (open circle) HiPCO nanotubes as well as air- and Ar-annealed and non-annealed arc-discharge samples (diamond). No obvious dependence on degree of doping is observed.

FIG. 6. (Color online) (a) Dependence of G^+ peak linewidth Γ on doping (varied by gate voltage, V_G) and calculated total dephasing time for narrowest linewidth for a single semiconducting nanotube (RBM at 135 cm^{-1} under 633 nm excitation) with no observable D-band. (b) Fitted Raman spectra at V_G = -0.3 V and V_G = -0.9 V, the narrowest and broadest spectra respectively. Overall fit in gray and components in blue. Simultaneous electrical/static Raman measurement conditions are described in Ref. 12.

FIG. 7. (Color online) (a) Normalized integrated TRIARS intensity (I/I_{max}) as a function of probe delay for HiPCO(0 mM) (black square) and HiPCO(100 mM) (red circle) samples with A_D/A_G of 0.21 ± 0.03 and 1.53 ± 0.17, respectively. (b) OP lifetime (T_1) dependence on relative defect concentration (i.e., A_D/A_G) for non-functionalized (square), functionalized (filled circle), and functionalized/PEI-doped (open circle) HiPCO nanotubes as well as arc-discharge samples (diamond). T_1 error bars are from least-squares curve fitting and A_D/A_G error bars are from variations measured at three different locations in each sample.

FIG. 8. (Color online) Influence of relative defect concentration, I_D/I_G (peak height ratio), on lifetime broadening, $(2\pi c T_1)^{-1}$, calculated from T_1 values measured by TRIARS and total linewidth of G^+ peak, Γ, of single semiconducting nanotubes from static Raman measurements. Lines are linear fits. Open squares correspond to linewidths of electrostatically gated single semiconducting nanotubes where charge neutrality is ensured.

FIG. 1

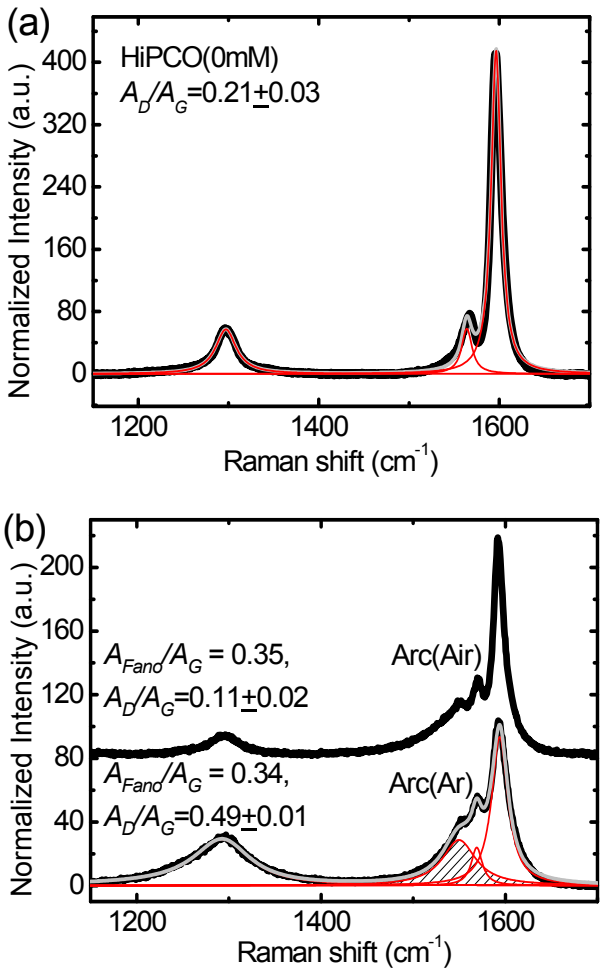
(a)
HiPCO(0mM)
A_D/A_G=0.21±0.03
Normalized Intensity (a.u.)
400
320
240
160
80
0
1200
1400
1600
Raman shift (cm^{-1})
(b)
A_{Fano}/A_G = 0.35,
A_D/A_G=0.11±0.02
Arc(Air)
A_{Fano}/A_G = 0.34,
A_D/A_G=0.49±0.01
Arc(Ar)
Normalized Intensity (a.u.)
200
160
120
80
40
0
1200
1400
1600
Raman shift (cm^{-1})

FIG. 2

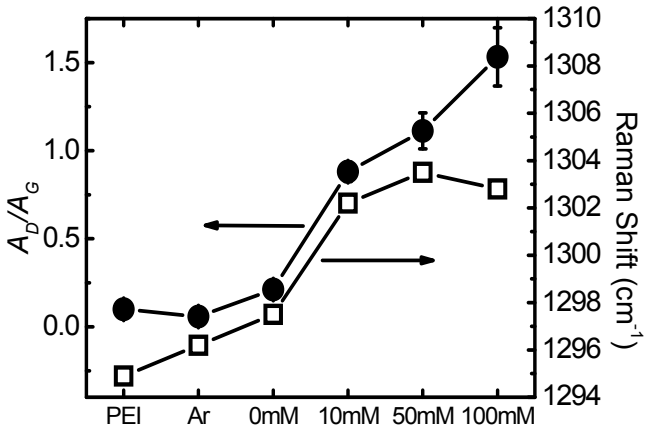
1.5
1.0
0.5
0.0
A_D/A_G
1310
1308
1306
1304
1302
1300
1298
1296
1294
Raman Shift (cm^{-1})
PEI
Ar
0mM
10mM
50mM
100mM

FIG. 3

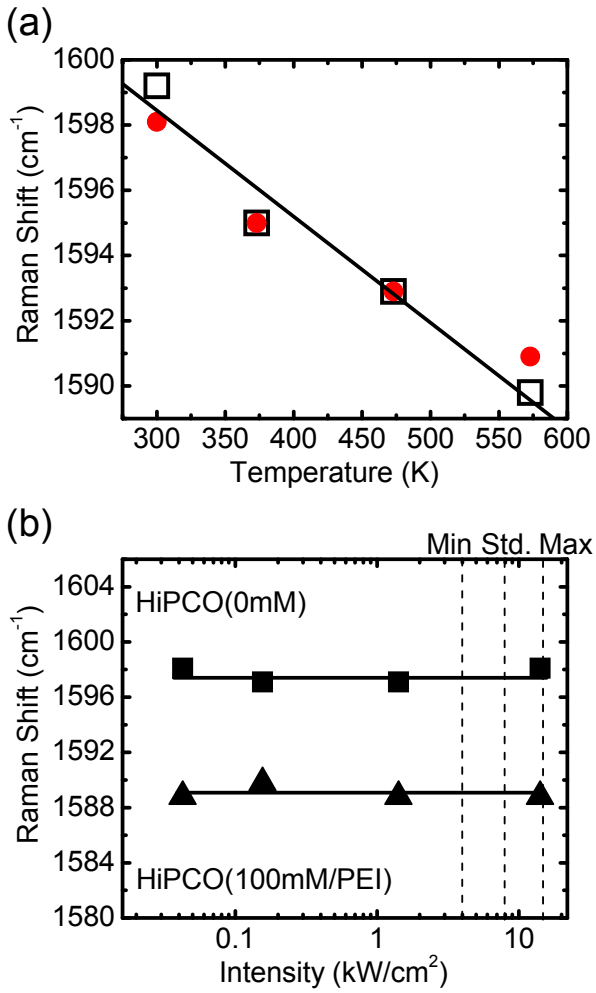
(a)
Raman Shift (cm-1)
1600
1598
1596
1594
1592
1590
300 350 400 450 500 550 600
Temperature (K)
(b)
Min Std. Max
HiPCO(0mM)
HiPCO(100mM/PEI)
Raman Shift (cm-1)
1604
1600
1596
1592
1588
1584
1580
0.1
1
10
Intensity (kW/cm2)

FIG. 4

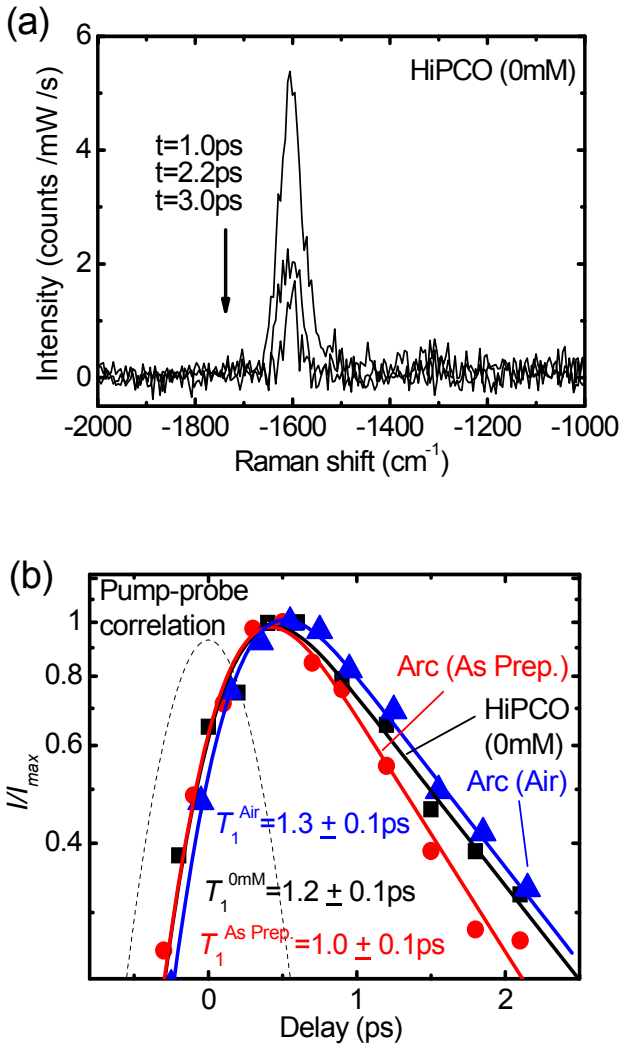
(a)
HiPCO (0mM)
t=1.0ps
t=2.2ps
t=3.0ps
Intensity (counts /mW /s)
Raman shift (cm-1)
(b)
Pump-probe correlation
Arc (As Prep.)
HiPCO (0mM)
Arc (Air)
T1 Air =1.3 ± 0.1ps
T1 0mM =1.2 ± 0.1ps
T1 As Prep. =1.0 ± 0.1ps
I/Imax
Delay (ps)

FIG. 5

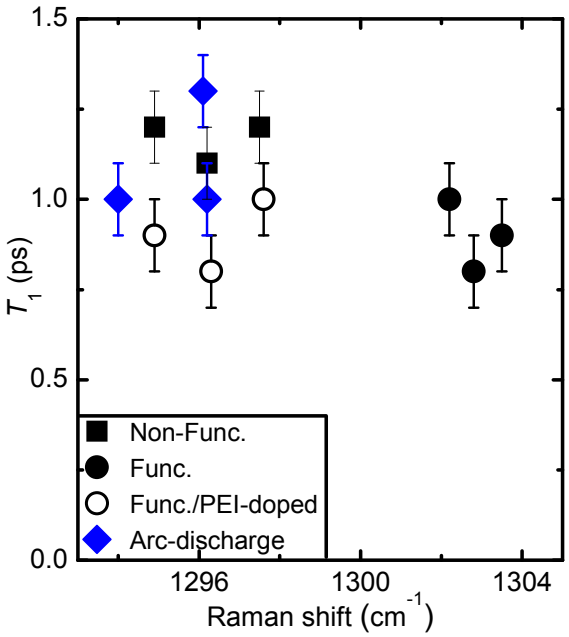
1.5
1.0
0.5
0.0
T_1 (ps)
1296
1300
1304
Raman shift (cm^{-1})
Non-Func.
Func.
Func./PEI-doped
Arc-discharge

FIG. 6

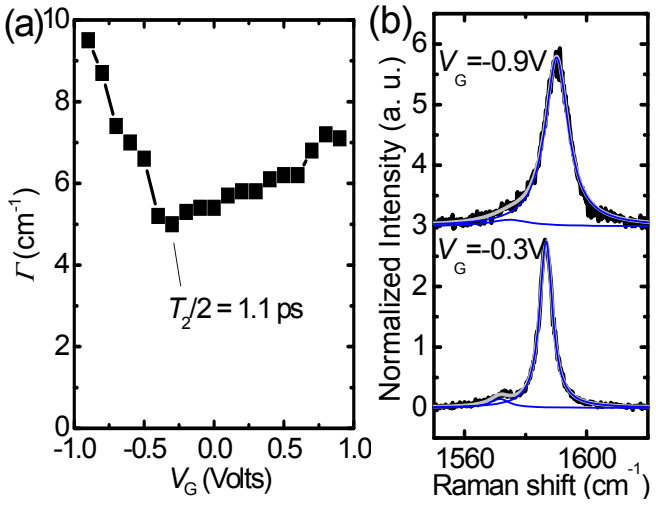
(a)
Γ (cm-1)
T2/2 = 1.1 ps
VG (Volts)
(b)
VG =-0.9V
VG =-0.3V
Normalized Intensity (a. u.)
Raman shift (cm-1)

FIG. 7

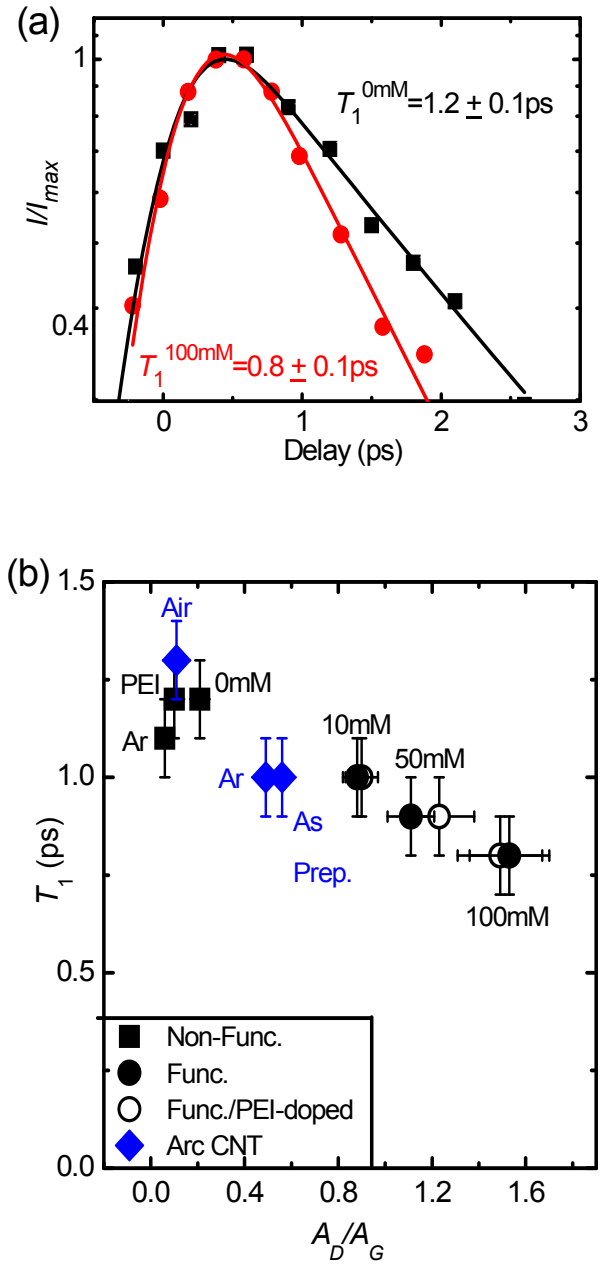
(a)
1
0.4
I/I_{max}
T_1^{0mM}=1.2 ± 0.1ps
T_1^{100mM}=0.8 ± 0.1ps
0
1
2
3
Delay (ps)
(b)
1.5
1.0
0.5
0.0
T_1 (ps)
Air
PEI
0mM
Ar
Ar
As
Prep.
10mM
50mM
100mM
Non-Func.
Func.
Func./PEI-doped
Arc CNT
0.0
0.4
0.8
1.2
1.6
A_D/A_G

FIG. 8